Journal of Alloys and Compounds 724 (2017) 841–850

Contents lists available at ScienceDirect

Journal of Alloys and Compounds

journal homepage: http://www.elsevier.com/locate/jalcom

Thermal recovery mechanisms of UO_2 lattices by defect annihilation

Seçkin D. Günay

Department of Physics, Faculty of Science, Yıldız Technical University, Esenler, 34210, İstanbul, Turkey

ARTICLE INFO

Article history:
Received 14 October 2016
Accepted 8 July 2017
Available online 11 July 2017

Keywords:
Uranium dioxide
Recovery
Fission
Alpha-particle
Interstitial defect

ABSTRACT

Previous investigations on the thermal recovery of irradiated uranium dioxide crystals defects related to each recovery stage have been estimated based on indirect observations such as activation energy calculations of ion migration during crystal lattice recovery. In this study, thermal recovery mechanisms for fission- and α-particle-irradiated uranium dioxide lattices were investigated by atomistic simulation methods. Isochronal and isothermal annealing methods were applied to the irradiated samples. Following reported procedures, the activation energies were calculated by molecular dynamics simulations and compared with empirical data, which showed good agreement with the experimental results. The migration energy barrier and the recovery energies of the obstruction type defects were calculated using molecular dynamics simulations and density functional theory. The irradiated crystal recovery stages are also discussed. Contrary to the reported predictions, direct, visual observation of the simulated data show that fission- and α-particle-irradiated crystals are not thermally recovered via the same mechanism. All the three recovery stages of the fission-irradiated uranium dioxide crystal are attributed to oxygen interstitials, while the first, second, and third recovery stages of the α-particle-irradiated crystals are attributed to oxygen–uranium, uranium, and uranium interstitial defects respectively. Finally, in a previous study of the present author it was shown that fission- and α-particle induced lattice swelling of uranium dioxide occurs due to obstruction-type defects. In this study, the main driving force of thermal recovery of irradiated crystals was once more observed as obstruction-type defects, which initiated all other types of defect recovery at each lattice recovery stage.

© 2017 Elsevier B.V. All rights reserved.

1. Introduction

In a previous study [1], molecular dynamics (MD) simulations were used to elucidate the swelling mechanisms of uranium dioxide crystals with irradiation-induced ingrowth of defects, and the data were compared with experimental results [2–4]. Investigation of fission- and α-particle irradiation-induced defects showed that lattice swelling was primarily caused by obstruction defects. These were oxygen ions for fission-irradiated, and uranium ions for α-particle-irradiated crystals.

In this study, the recovery mechanisms for the damaged uranium dioxide crystals investigated in the previous research [1] were examined by both molecular dynamics and density functional methods. Since time and temperature have a great influence on the damaged crystals, the isochronal and isothermal lattice parameter recovery behaviours were investigated and compared with the experimental results. There is agreement between empirical and theoretical results. Each demonstrated three recovery stages and activation energies were obtained for each stage. The presence of defects at each recovery stage in the experimental groups and the appreciable extent of agreement implied that the first, second, and third recovery stages were influenced by oxygen interstitials, uranium vacancies, and helium ions trapped in vacancies, respectively [5–8]. In this work, the recovery stages were observed and the main driving force for lattice recovery at each stage was due to obstruction defects, which initiate the recovery process.

In alpha-particle-irradiated crystals, as the interstitial uranium defects combined with the uranium vacancies, highly distorted oxygen ions also migrated to their normal positions. Consequently, both oxygen and uranium ions were recovered in the first stage. In the second and third stages, interstitial uranium ions were recovered. Considering the empirical and simulation data, oxygen migration in the first stage and helium migration in the third stage are presumably a corollary of uranium defect recovery.

Contrary to the proposed mechanism of experimentalists, in the fission-irradiated uranium dioxide crystals, oxygen interstitials

E-mail address: sgunay@yildiz.edu.tr.

http://dx.doi.org/10.1016/j.jallcom.2017.07.100
0925-8388/© 2017 Elsevier B.V. All rights reserved.

were recovered in all stages. During recovery, the migration energy, the energy change per obstruction type defect, and the lattice parameter change were calculated by two computational methods: classical molecular dynamics and first-principle methods. Both results were compared and are in agreement.

To clarify the terminology used in this study, the uranium obstruction defects are at an octahedral position surrounded by six uranium ions, and oxygen obstruction defects are surrounded by four uranium and four oxygen ions. These obstruction defects obstruct the ⟨110⟩ channel and the distortion defects are distorted into the ⟨110⟩ channel. Terminology is used because when the defect concentration is so high, all interstitial defects in crystal do not have constant number of ions surrounding them and some have unstable positions which is called distortion type. These may also accumulate as clusters. In other words, all interstitial defects are not obstruction type defects.

2. Computational methods

2.1. Density functional theory calculations

Density functional theory was used to calculate the ground state energies, forces, and structures of defected (Uranium Frenkel pair) and defect-free UO_2 crystals. These calculations were performed using the projector augmented-wave (PAW) method, which was implemented in the Vienna *Ab initio* simulation package (VASP). The UO_2 system possesses localised (strongly correlated) $5f$ electrons, which should not be computed using the same method as delocalised electrons, especially if this method exposes delocalised electrons to an average Coulomb potential. Strong Coulomb repulsion exists between localised f electrons; thus, the Hubbard term U was included in the calculations. DFT + U methods were used instead of the traditional DFT methods when onsite interactions (between electrons localised on the same atomic center) need to be described.

A generalised gradient approximation (GGA) was chosen for the exchange-correlation approximation. The Hubbard parameters were $U = 4.5$ eV and $J = 0.51$ eV, as in previous studies [9–11]. The cut-off energy of the plane wave was 500 eV. A $2 \times 2 \times 2$ Monkhorst-Pack k-point mesh was used for the sampling of the irreducible Brillouin zone. The supercell contained eight unit cells ($2 \times 2 \times 2$) with 96 atoms ($U_{32}O_{64}$).

The UO_2 unit cell has a CaF_2 structure with an Fm-3m space group. In order to simulate a uranium Frenkel pair, a uranium ion was moved from its normal site to an interstitial position, which is called an obstruction defect. This point is surrounded by six uranium ions where the interstitial ion is equidistant from the other six uranium ions.

2.2. Molecular dynamics simulations

Newton's equations of motion were solved iteratively for each particle in the supercell. Two types of potential models were used in this study: a pair potential that was proposed by Yakub et al. [12], and a pair potential with the many-body embedded atom model (EAM) that was proposed by Cooper et al. [13].

The interaction for the first potential between particles i and j is,

$$\varphi_{ij}(r_{ij}) = \frac{Z_i Z_j}{r_{ij}} + A_{ij} e^{-r_{ij}/\rho_{ij}} - \frac{C_{ij}}{r_{ij}^6} + D_{ij}\left(e^{-2\beta_{ij}\left(r_{ij}-r_{ij}^0\right)} - 2e^{-2\beta_{ij}\left(r_{ij}-r_{ij}^0\right)}\right) \quad (1)$$

The first term is the long-range Coulomb interaction between i and j, and Z is the ionic charge of the species. The electrostatic portion of the equation is calculated by the Ewald method where the cut-off distance is set at 10 Å. The remaining terms describe short-range interactions: the second and third terms are the Buckingham potentials, and the fourth term is the Morse potential. The parameters were developed by Yakub et al. [12] and clarified by Devanathan et al. [14]. The Beeman algorithm was employed for the integration of Newton's equations. To determine the initial kinetic energy, a Maxwell-Boltzmann distribution was used to assign velocities to each ion at the desired temperature. The initial configuration gives an excess potential energy, which leads to an overestimation of the kinetic and potential energies. In order to avoid such a problem, the system was equilibrated for 30 ps with a 1 fs time step. The physical properties were not determined herein and they were calculated starting from the end of the first part for 70 ps. The total simulation time was 100 ps; in subsequent simulations, the time was initially increased to 500 ps and finally to 10,000 ps. Temperatures of all systems were increased from 300 K to 3200 K with a 50 K interval.

NPT ensemble was applied to the system with the MOLDY program [15]; P is the Parinello-Rahman compatible constant pressure method where the system is constrained by a uniform-dilation, and T is the constant temperature ensemble, which means the system is coupled to a heat bath using the Nose-Hoover method.

The second interaction potential [13] comprises two components, which are the pair-wise and many-body components. The total simulation time was 100 ps and the cut-off distance was 11 Å [16]. The details of the simulation parameters were described by Cooper et al. [13].

An $8 \times 8 \times 8$ supercell box was used, which contained 2048 uranium and 4096 oxygen ions. Defected samples were prepared following the procedure reported in a previous study [1]. Defected layers were prepared by moving cations or anions from their normal positions to interstitial sites. These are called as initial Frenkel pairs and these are not placed in successive layers otherwise they directly terminate one another. A sample figure of a supercell with 60 uranium IFP is displayed in Fig. 1.

The average number of defects was calculated with the following expression in the Δr range around a central ion.

$$\overline{M_\alpha} = \frac{\sum_{i=1}^{n_t} \sum_{j=1}^{N_\alpha} K_{ij}}{n_{\alpha\beta} n_t} \quad (2)$$

M_α is obtained by averaging the defect numbers over the number of time steps, n_t. K_{ij} represents the number of β ion around

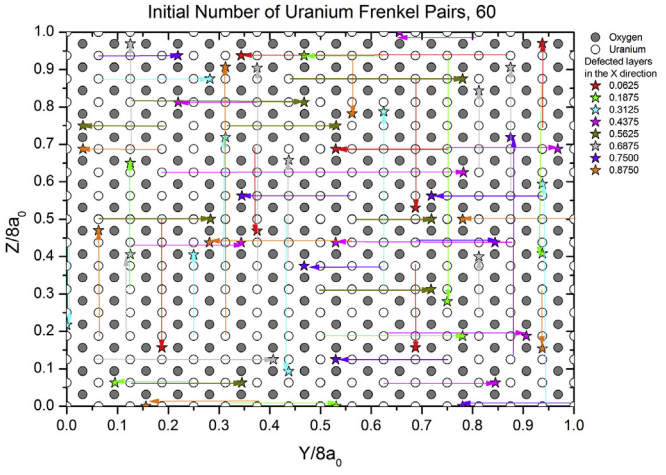


Fig. 1. A sample of a supercell with 60 uranium IFP.

the jth α ion during the ith time step within the range Δr. $n_{\alpha\beta}$ is the first coordination number of the perfect crystal [1]. The Δr interval was chosen from the radial distribution function depending on the defect under study: obstruction/distortion and uranium/oxygen defects. For example, uranium obstruction defects were calculated from Fig. 2 where Δr ≅ 3.35–0.0 and were calculated as $\overline{M_U^{obs}} \cong 44.9$.

Unlike distortion defects, obstruction defects have well-defined boundaries in the radial distribution function (Fig. 2). The oxygen obstruction defect is not visible in Fig. 2 but will be discussed in the following sections.

3. Results

In a previous study [1], it was concluded that fission irradiation of UO_2 gave oxygen defects and irradiation with α-particles gave both uranium and oxygen defects. As the defects were created, a linear dependence of the relative lattice expansion on the number of obstruction defects was observed. During fission irradiation, these obstruction defects were oxygen interstitials, and during α-particle irradiation, they were uranium interstitials.

3.1. Isochronal annealing

3.1.1. Supercells with oxygen Frenkel pairs

Nakea et al. irradiated UO_2 single crystals with fission [2,3] and observed a lattice parameter change (Fig. 3a inset). As the number of initial oxygen Frenkel pairs (IFP) increased, the lattice parameter increased to a saturation value, and the experimental data agreed with the simulated data for a 5 × 5 × 5 supercell [1]. In this study, MD simulations were re-performed for an 8 × 8 × 8 UO_2 supercell for the two interaction potentials at 300 K (Fig. 3a). Nakea et al. observed two stages up to the highest data point and these stages can also be observed in the simulated data. Here, the highest data point should be near 80 IFP in Fig. 3a.

Nakea et al. [5] performed a thermal recovery experiment for the fission-irradiated UO_2 sample (Fig. 3b). They suggested the first recovery stage be attributed to the migration of oxygen vacancies and the second stage to uranium vacancies. Other studies [17,18] suggested that the first stage should be because of the migration of oxygen interstitials. Similar stages are observed with the MD simulation in both samples in the present study (IFP 40 and IFP 80), and the total recovery temperature is about 900 K, which is in agreement with the experimental data. The annihilation of oxygen Frenkel pairs is, therefore, the mechanism of recovery in fission-irradiated UO_2 crystals. These oxygen ions are obstruction defects, surrounded by four oxygen and four uranium ions. Very small changes (Δa ≈ a_o 10^{-4}Å) were observed in the MD simulation lattice parameter data as the IFP was increased. Clearer and more resolved peak points with less scattered data can be observed with bigger supercells and by collecting more data points in the MD simulations of Fig. 3. The equidistant jumps of the Yakub et al. potential lattice parameter data are from the MD program precision limits [15]. These equidistant jumps of data in y axis were not observed with the Cooper et al. potential in Fig. 3a because the other MD program [16] have higher precision. In the following section, such a high precision was not necessary because lattice expansion with α-particle irradiation is nearly ten times larger than that with fission irradiation.

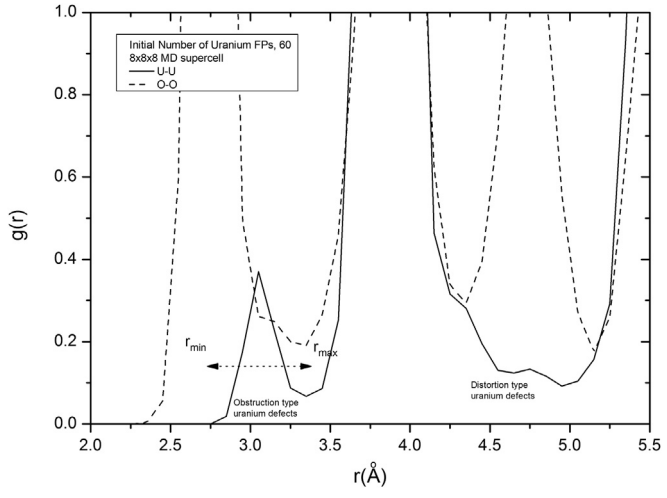


Fig. 2. The radial distribution function of the supercell with 60 uranium IFP after equilibrium.

3.1.2. Supercells with uranium Frenkel pairs

Weber irradiated a UO_2 single crystal with α-particles [4] and an exponential growth of the lattice parameter was observed (Fig. 4a inset). A correlation between the relative changes in the experimental lattice parameter of UO_2 (from the α-irradiation dose) and the MD simulated lattice parameter (from the increase of uranium IFP defects (Fig. 4a) has been demonstrated [1]. It should be emphasized that introducing uranium IFP defects only does not mean α-particles can only effect uranium sublattice but not oxygen sublattice. It will be demonstrated throughout the article that uranium defects have driving effect and give form the oxygen sublattice. For this reason introducing the oxygen defects beside uranium defects have no impact.

Another point, lattice swelling was mainly due to the uranium FP obstruction defects (interstitial uranium ions located at octahedral sites) and showed a linear dependence on it. In other words, as the number of uranium FP obstruction defects increased, the lattice parameter changed linearly until a saturation point was reached [1].

Weber also investigated the recovery of an alpha-particle-irradiated UO_2 single crystal by increasing the temperature. Three recovery stages were observed in this experimental study at 573 K, 848 K, and 1198 K (Figs. 4b and 5). Weber also found that the total recovery occurred near 1323 K [6]. Weber considered the region above 1323 K, where $\Delta a/a_o = 0.06\%$, as the region of total recovery of the crystal. This $\Delta a/a_o$ value used by Weber to mark the total recovery boundary was used to determine the point of crystal total recovery in the simulated results.

Similarly to Weber's work, this work focuses on the recovery behaviour of the lattice parameter and defects associated with increases in temperature, by using isochronal and isothermal annealing.

In Fig. 4b, the lattice parameter recovery of each sample (supercells with different populations of uranium IFPs) against the temperature demonstrates an isochronal recovery. Isochronal recovery data points were obtained from 100 ps simulations. The recovery steps are not evident owing to data scattering; however, total recovery can be determined and occurs near 2400 K–2600 K ($\Delta a/a_o = <0.06\%$). The simulation overestimated the experimental value by nearly 1000 K.

Time is an important variable for recovery. To improve the results, the simulation time was increased to 500 ps, which reduced data scattering and resulted in well-defined recovery stages. Moreover, increasing the total simulation time reduced the overestimation of the experimental results, and resulted in better agreement with the experimental value (Fig. 5). The total recovery temperature of all samples was reduced by 200 K–400 K and was between 2000 K and 2400 K for the 500 ps simulation time.

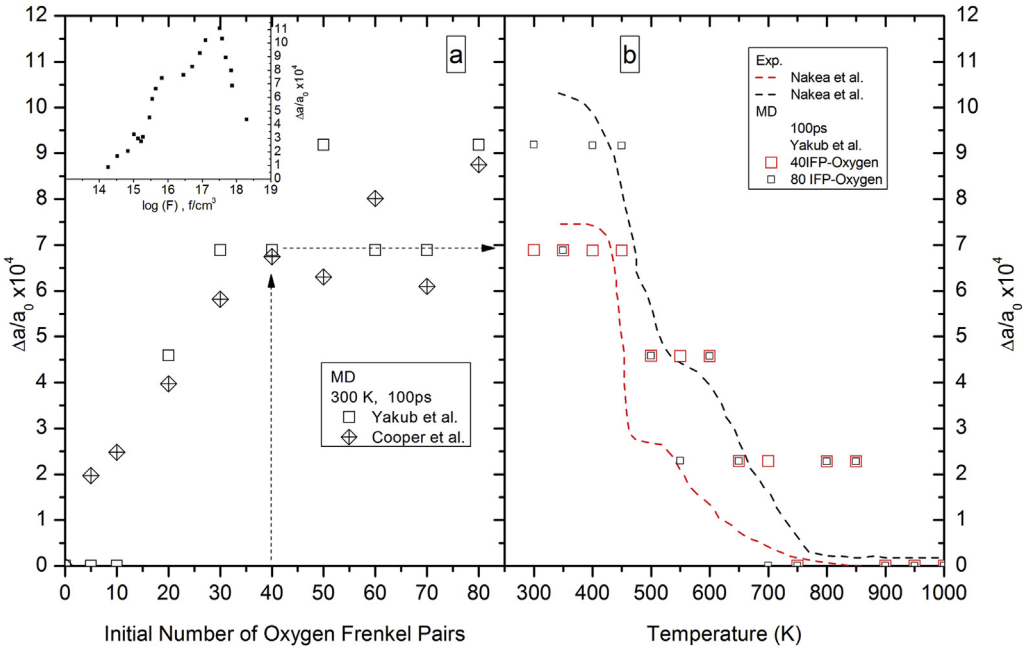


Fig. 3. The MD simulation results compared with the experimental data collected by Nakea et al. [5,8] a) The relative lattice increase of UO_2 with increasing number of oxygen IFPs. b) The thermal recovery of the UO_2 lattice for 40 and 80 oxygen IFPs.

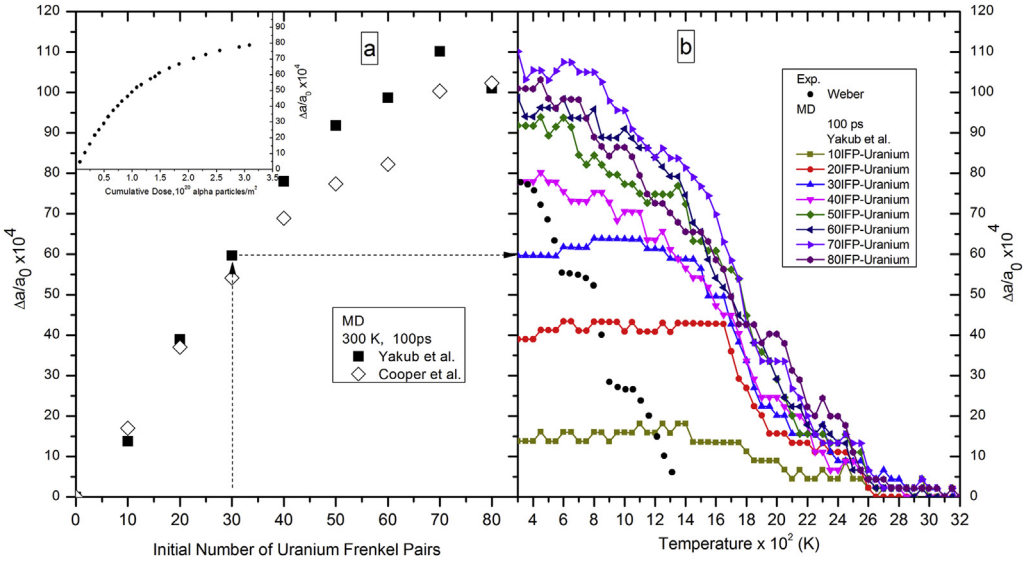


Fig. 4. The MD simulation results compared with Weber's experimental data [4,6] a) The relative lattice increase of UO_2 with increasing number of uranium IFPs. b) The thermal recovery of UO_2 lattices for each number of uranium IFP.

However, if the time is increased sufficiently, values near the experimental results are likely to be obtained, which could lead to a false positive. Main reasons of the deviation of simulation from experimental results are insufficient interaction potentials or other reasons specific to the molecular dynamics methods. For this reason, in order to simulate a given experiment, increasing the simulation time uncontrollably is not recommended for determining the temperature of recovery stages. One should increase the time considering the defect concentration (or lattice parameter) both in the simulation box and experimental sample simultaneously. The stage levels in Fig. 6 could indicate the relevant recovery time for the simulation.

In Fig. 6, the stage locations from the simulated results are indicated for all samples and are not well defined. For 20 IFP sample, there are two stages, and for the 40 and 70 IFP samples, there are three stages. The temperatures for all stages were overestimated; however, the stage levels, relative lattice expansion (y-axis data) are quite close to experimental values.

Weber observed that the second stage recovery was much sharper than the others were, and concluded that there was a distribution in activation energies in the first and third stage but only one activation energy value was observed for the second stage. In the MD simulation, the second stage also displays a sharp decrease.

In Fig. 6, the recovery stage coordinates are difficult to determine, so the derivative of the smoothed data of IFP70 (Fig. 7a) is

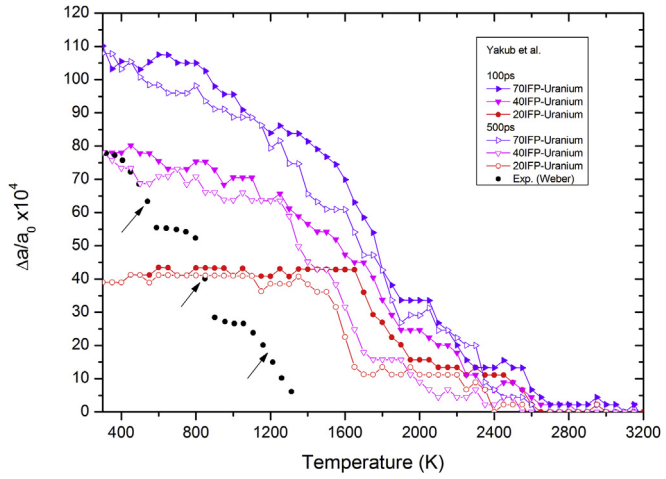


Fig. 5. A comparison of the MD simulation results for the UO_2 lattice thermal recovery for 100 ps and 500 ps simulation time scales. The arrows indicate the experimental thermal recovery stages.

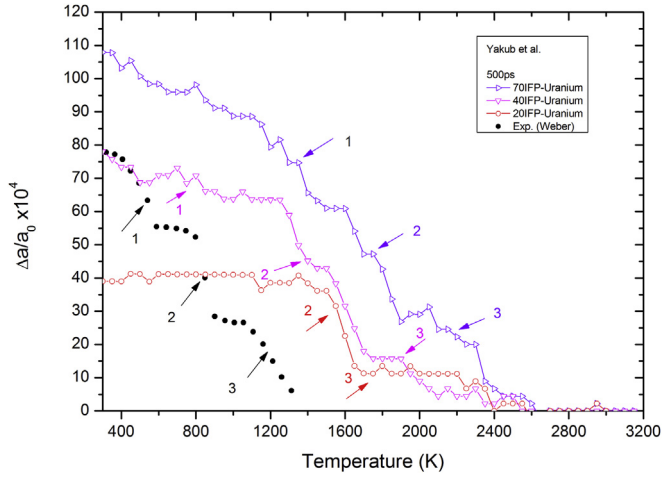


Fig. 6. The recovery stages of the MD simulations and the experimental results.

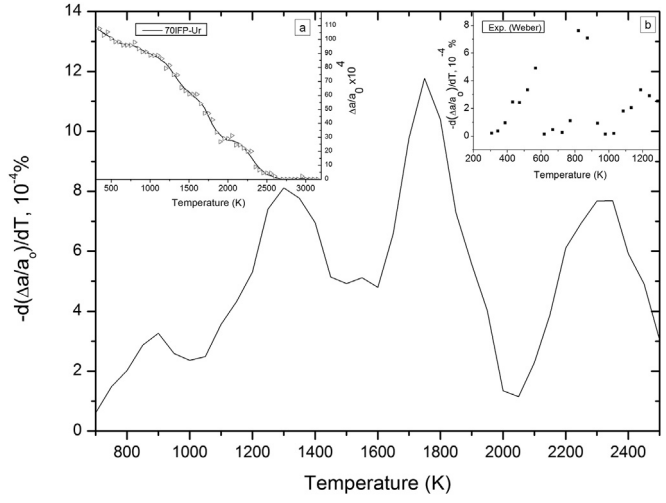


Fig. 7. The first derivative of inset a. a) Smoothed data of the relative lattice changes of 70 uranium IFP with temperature b) The first derivative of the experimental data.

plotted in Fig. 7. From the derivative, the recovery stages are at 1300 K, 1750 K, and 2300 K. The recovery stage temperatures are used in the next section to determine the activation energies from the isothermal data. There is also a pre-peak at 900 K prior to the first stage. In Fig. 7b, a similar peak can be observed in Weber's data near 450–500 K, which was not discussed in the study.

3.2. Isothermal annealing

Isothermal annealing was applied to the 70 IFP samples: at 1300 K and 1400 K for the first stage, and at 1750 K and 1800 K for the second stage. Each simulation was performed for 10,000 ps (10 ns) and started from the preceding 50 K lower, 100 ps run. The data was smoothed by the adjacent averaging method to reduce data noise from random error. The isothermal recovery data decreases exponentially in all cases. Similarly to the experimental results (inset Fig. 8), at low temperatures the exponential decay rate is small but increases with temperature (Fig. 8).

The cross-cut method [19] was applied to the simulated data in Fig. 8. Parallel lines to the x-axis were drawn at random levels where t and T values were obtained. The ln (t) versus 1/T was plotted and Eq. (3) was implemented.

$$\ln(t_1/t_2) = E\Big/k\left(T_1^{-1} - T_2^{-1}\right) \tag{3}$$

This procedure was applied to the first and second stages, where the activation energies were calculated as 1.85 eV and 4.0 eV respectively. Experimental calculations following this method gave activation energies of 1.5 eV and 2.2 eV respectively [6].

Weber also determined the activation energies by using a method proposed by Primak [20–22], using Eq. (4).

$$E_0 = kT\ln(Bt) \tag{4}$$

Weber assumed a constant value for the frequency factor B $\approx 10^{10}$ s^{-1} at all stages; t is the time taken for the Weber's experiment (30 min), k is the Boltzmann constant, and E_0 is the mean activation energy, which corresponds to the temperature for maximum recovery in each stage under isochronal annealing. The annealing times were very small compared to the experimental values in our simulation, so the frequency factor was altered. In Primak's work [20], the frequency factor was B $\approx 10^{14}$ s^{-1} for the simulation time scale and was assumed constant over all stages. The activation energies calculated using this method for the first,

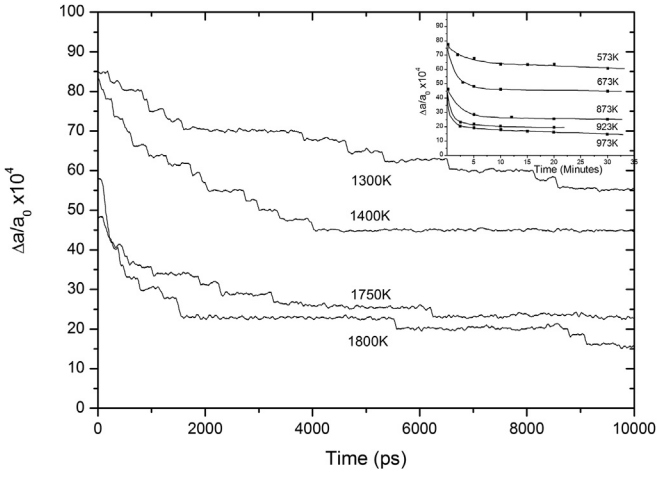


Fig. 8. Isothermal annealing applied to the 70 uranium IFP supercell at the temperatures of the first and second stages. The inset is Weber's experimental results [6].

second, and third stages were 1.5 eV, 1.945 eV, and 2.55 eV, respectively, whereas Weber found values of 1.5 eV, 2.2 eV, and 3.1 eV, respectively.

3.3. Interstitialcy migration mechanism of uranium

The MD simulation method and first-principle DFT calculations were performed to observe and identify the interstitialcy (indirect interstitial) mechanism of uranium in the alpha-particle-irradiated crystal. The energy barriers and relative energy change during recovery were calculated from these methods.

3.3.1. MD simulation

The indirect interstitial migration mechanism of the interstitial uranium defect (obstruction) was observed throughout the MD simulation, at all temperature ranges.

Fig. 9 depicts the ⟨110⟩ view (slightly tilted about the y-axis) of the UO_2 crystal lattice. The oxygen ions were removed from the figure for clarity. All uranium ions are at their normal sites except the interstitial uranium ion at site A, which blocks one of the channels between rows of uranium ions. The two ions at the top left of the octahedron are displayed to indicate the position of vacancy site C. As indicated in Fig. 10, near 5000 ps, the interstitial uranium ion at site A moves to site B and pushes the uranium ion at site B towards site C, which demonstrates an interstitialcy mechanism for recovery (Video 1).

Supplementary video related to this article can be found at http://dx.doi.org/10.1016/j.jallcom.2017.07.100.

The volume occupied by the octahedron decreases after recovery. This change can be observed between the left-hand side (before recovery) and the right-hand side (after recovery) of Fig. 9. Concurrently in Fig. 10, the lattice parameter at 300 K near 5000 ps decreases and recovers towards a perfect crystal lattice parameter, where the change in the lattice parameter is $\Delta a = a_{after} - a_{before} \approx -9.865 \times 10^{-4}$ Å. Similar lattice recovery steps are observed in Fig. 8 at higher temperatures. The total crystal lattice energy change is $\Delta E = E_{after} - E_{before} \approx -10$ eV, which indicates that the supercell is in a more favourable state after recovery. These energy and lattice differences correspond to only one interstitialcy recovery of a uranium ion.

3.3.2. DFT method

The uranium defect recovery by the interstitialcy mechanism was investigated by DFT. The interstitial (direct interstitial) migration mechanism was not considered because the interstitialcy mechanism was observed in all MD simulations. The initial and final DFT structures were considered from the recovery mechanism of the initial and final structures from the MD simulation (similar to Fig. 9). In the initial structure, the interstitial uranium is located in the octahedral site with a nearby uranium vacancy. The final structure corresponds to the defect-free crystal. The atomic structure and the cell shape were optimised for the initial and final states with VASP [23–25]. The climbing image NEB method (CI-NEB) was applied to find the saddle point [26].

The migration energy was calculated more accurately with CI-NEB than with regular NEB methods because the energy saddle point is found without interpolation of energy. A generalised solid-state NEB method [27] was also used, because initial and final structures have different cell sizes, and this method allows changes in the lattice vectors within the end-points. The calculated migration energy barrier was 0.67 eV and the energy difference before and after the recovery process was $\Delta E = E_{after} - E_{before} = -9.69$ eV, which agrees with the MD simulation result, −10 eV (Figs. 11 and 12). Finally, in this context, first-principles calculations of uranium diffusion in uranium dioxide was also investigated by Dorado et al. [28] and used NEB method to calculate migration energies.

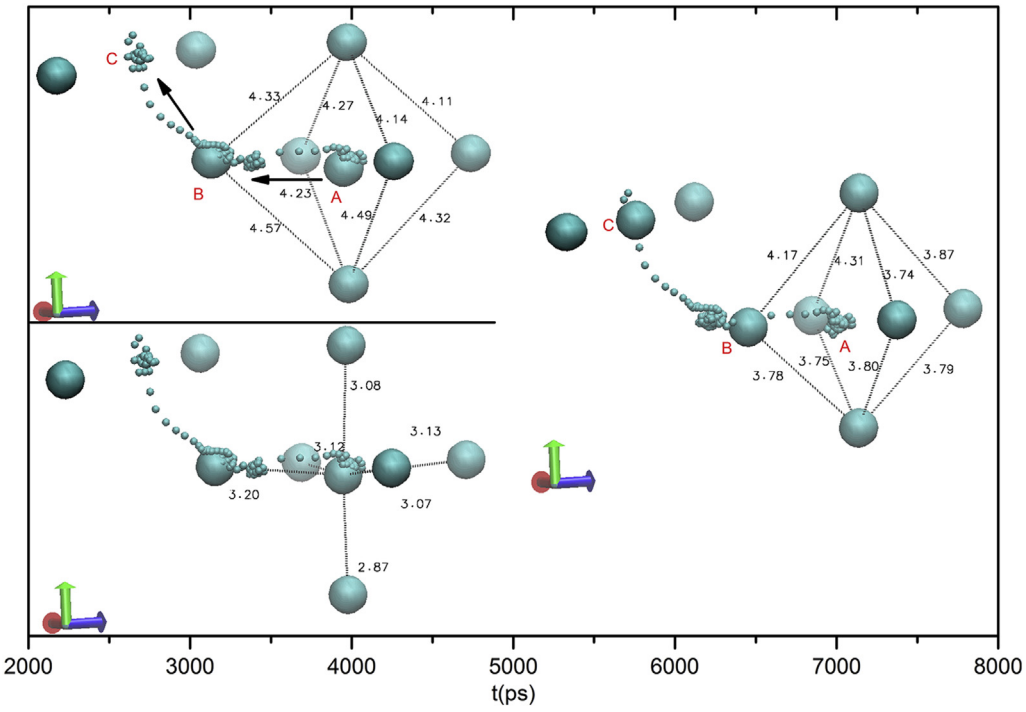


Fig. 9. The ⟨110⟩ views before and after the recovery of the interstitial uranium defect at the octahedral position. The uranium ions are colored in cyan and the oxygen ions are removed from the figure for clarity. At about 5000 ps, recovery occurs by an interstitialcy mechanism. (For interpretation of the references to colour in this figure legend, the reader is referred to the web version of this article.)

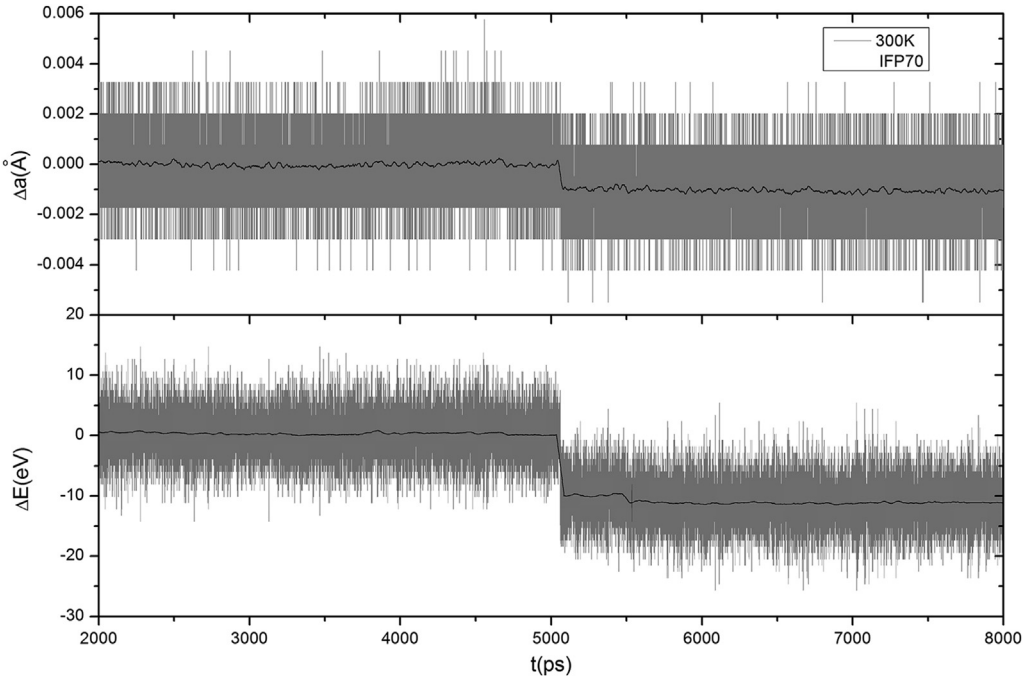


Fig. 10. The change in the lattice parameter and energy with time. At about 5000 ps, recovery occurs by an interstitialcy mechanism.

3.4. Interstitialcy migration mechanism of oxygen

The MD simulation method was performed to observe and identify the interstitialcy mechanism of oxygen in the fission-irradiated UO_2 crystal. The energy and lattice parameter change during recovery were calculated with this method. The indirect interstitial migration mechanism was observed throughout the MD simulations, at all temperature ranges.

Fig. 13 depicts a ⟨110⟩ view of the UO_2 lattice where the uranium ions are colored in cyan and the oxygen ones are colored in blue. All uranium and oxygen ions are at their normal sites except the interstitial oxygen ion at site A, on the left-hand side of the figure, which blocks the channel between rows of uranium and oxygen ions in the ⟨110⟩ direction. The interstitial oxygen ion is surrounded by four oxygen and four uranium ions. As indicated in Fig. 13, after 70 ps, the interstitial oxygen ion at site A moves to site B and pushes the oxygen ion at site B towards site C, which demonstrates an interstitialcy mechanism of recovery (Video 2, Video 3, Video 4). Unlike the uranium ions, the positions of the oxygen ions at their normal sites changed slightly after recovery because the oxygen ions at interstitial positions can only push other oxygen ions outwards. The uranium ions are not affected by the interstitial oxygen ions and they remain in position. The effect of the interstitial oxygen ions was observed by measuring the distances of the diagonal uranium and oxygen ions, as shown in Fig. 13.

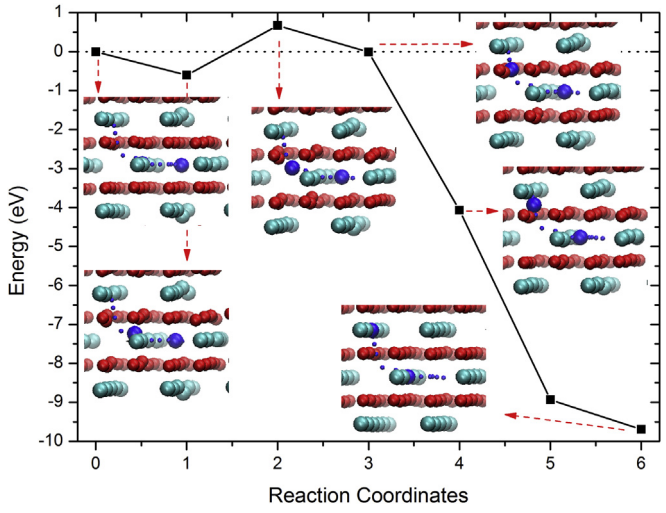


Fig. 11. The relative system energy calculated by Cl-NEB as the uranium ion migrates via an interstitialcy mechanism. The uranium and oxygen ions are colored in cyan and red, respectively. Two uranium ions are colored in blue to emphasize the interstitialcy (indirect interstitial) mechanism. (For interpretation of the references to colour in this figure legend, the reader is referred to the web version of this article.)

Supplementary video related to this article can be found at http://dx.doi.org/10.1016/j.jallcom.2017.07.100.

In Fig. 14, the lattice parameters and energies are seen before and after the interstitial oxygen recovery, which is demonstrated in Fig. 13. In the 80 IFP oxygen supercell at 300 K, recovery occurs at 70 ps, where the lattice parameter change is $\Delta a = a_{after} - a_{before} \approx -3.00578 \times 10^{-4}$ Å, and the crystal lattice energy change is $\Delta E = E_{after} - E_{before} \approx -5.89$ eV.

4. Discussion

In a previous study [1], swelling mechanisms of uranium dioxide lattices were investigated, mainly the lattice parameter swelling mechanisms owing to radiation-induced defect ingrowth from fission irradiation [2] and α-particle irradiation [4]. Moreover, the large difference (nearly an order of magnitude) of the relative lattice expansion data between these two experiments was also investigated. Reliable answers were found with MD simulations. Series of MD simulations were performed for 100 ps at 300 K with manually created oxygen and uranium Frenkel pairs in uranium dioxide crystal supercells. Simulations with gradually increasing number of Frenkel pairs were compared with both fission- and α-particle-irradiated samples experimental results, and showed that the molecular dynamics swelling data with ingrowth of uranium

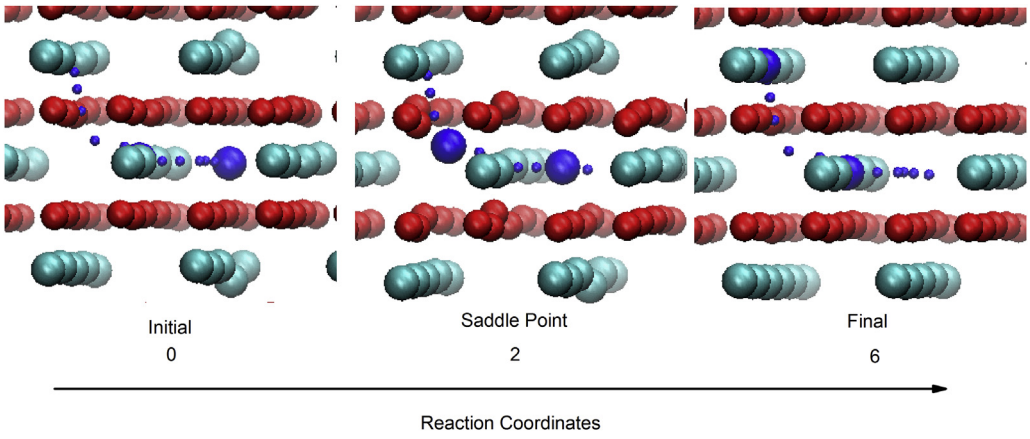


Fig. 12. The initial, saddle and final ⟨110⟩ views of the UO_2 supercell calculated using DFT. The uranium and oxygen ions are colored in cyan and red, respectively. Two uranium ions are colored in blue to emphasize the interstitialcy (indirect interstitial) mechanism. (For interpretation of the references to colour in this figure legend, the reader is referred to the web version of this article.)

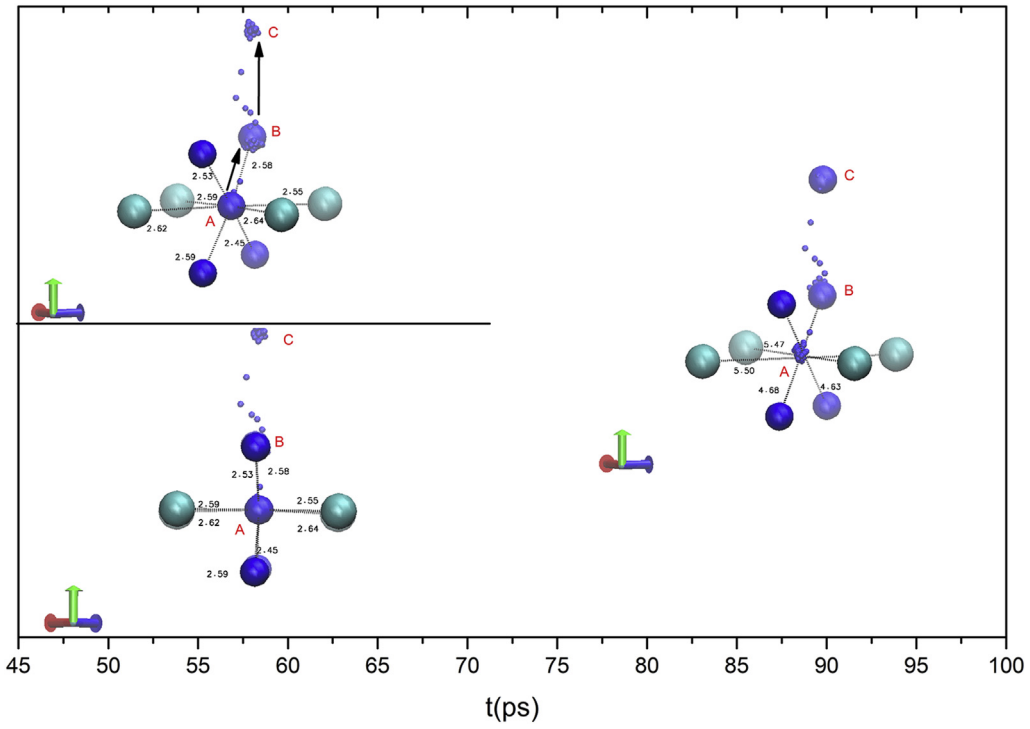


Fig. 13. The ⟨110⟩ views before and after recovery of the interstitial oxygen defect. The uranium and oxygen ions are colored in cyan and blue, respectively. At about 70 ps, recovery occurs by an interstitialcy mechanism. (For interpretation of the references to colour in this figure legend, the reader is referred to the web version of this article.)

dioxide IFPs resemble the experimental crystal swelling as the irradiation doses were increased. In addition, in this study, this behaviour was tested with a newly proposed potential, with an embedded atom model for uranium dioxide [13], and results were verified. MD simulations performed with the potential models proposed by Yakub et al. [12] and Cooper et al. [13] clearly showed that the swelling from fission irradiation was caused by the obstruction oxygen ions (oxygen surrounded by four oxygen and four uranium ions), and the swelling from α-particle irradiation was caused by the obstruction uranium ions (uranium at the octahedral position).

After verifying the data from previous work, the lattice recovery with temperature was investigated through MD simulations, and again, the number of obstruction defects was found to be the only reason for the lattice recovery. The experimental lattice recovery data from Nakea et al. [5] and Weber [6] were in agreement with the MD results. However, the α-particle-irradiated UO_2 crystal recovery temperature points from MD simulation were overestimated by nearly 1000 K (x-axis, Fig. 4). When the simulation time was increased from 100 ps to 500 ps, the simulated results were in much better agreement and the overestimation was reduced by 600 K (Fig. 6). This result showed that the simulation time has a great impact on the recovery temperature point. Extending the simulation time does not, however, necessarily lead to better results, because the recovery stages of the relative lattice expansion (y-axis, Fig. 6) should also be considered. The results at 500 ps were in agreement with the experimental results; therefore, 500 ps was considered an appropriate time scale estimation for MD

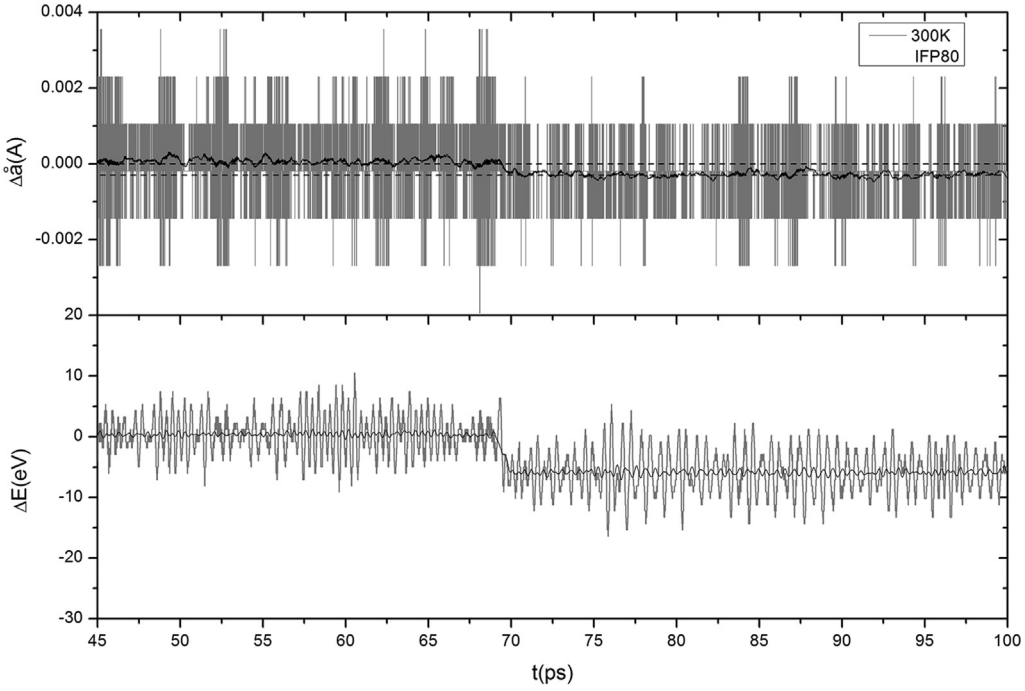


Fig. 14. The change in the lattice parameter and energy with time for recovery of the interstitial oxygen. At about 70 ps, recovery occurs by an interstitialcy mechanism.

simulations to compare with experimental time scale results in Fig. 6. In Fig. 8, the MD simulations and experimental results were compared, and time scales between these microscopic and macroscopic systems were 10 ns and 30 min, respectively. Obviously, the difference in the time scales was owing to the sample size (size of the pellet and simulation box). The defect concentration inside these boundaries or the relative lattice expansion should, therefore, be considered when determining the simulation time that corresponds to experiment. The acceptable time scales could be safely determined when these values are close to the experimental data.

In Nakea et al. [5] and Weber's [6] work, the sub-lattice ion responsible for each recovery stage was discussed. Weber found no direct information to associate a defect with each recovery stage but attributed the first stage to oxygen migration, the second stage to the uranium vacancies and the third stage to the helium release which were trapped in vacancies [6]. Despite the large difference in the relative lattice expansion data between α-particle- and fission-irradiated UO_2 crystals and Weber emphasize this situation, even so agreed with Nakea et al. [5] on the recovery procedure, where the α-particle- and fission-irradiated UO_2 crystal recovery procedures were similar. Further discussions and investigations have been considered, but their hypothesis is still valid for some actinide oxides up to now [7].

Our results show that the fission-irradiated crystals only exhibit oxygen defects and that the oxygen interstitials migrate towards the oxygen vacancies by an interstitialcy mechanism. During this migration, oxygen ions displace others toward an oxygen vacancy site, and two, three and sometimes even more oxygen ions (Video 4) can be involved in one indirect migration event. In Video 4, three oxygens are involved in one interstitialcy event. Our results does not comply with Nakea et al. study [5].

Alpha-particle-irradiated crystals have oxygen and uranium defects. As mentioned previously, the lattice expansion is caused by obstruction type uranium ions, and, naturally, these ions drive the recovery. There is, however, a smaller concentration of uranium defects than oxygen defects in the crystal; therefore, for the first stage of recovery, as one uranium ion is recovered by an interstitialcy mechanism, two or three oxygen ions migrate to their normal sites as well. This event can be elaborated as follows; in a previous study [1], the relative lattice change with the number of uranium obstruction defects demonstrated a linear dependence however, above a critical point, slope of the linear data is increased because at that point, oxygen ions are too distorted (because too much uranium defects exists) which results some of them remain as clusters and a portion of them penetrate into the interstitial uranium ion octahedron cage. Latter event augmented the gradient of the linear data. In this study, it is shown that, as the uranium ions are recovered, the cluster oxygens and trapped oxygens in the octahedral cage are also recovered (Video 5, Video 6, Video 7). In Video 5, eight oxygen defects, two trapped (pink) and six distorted (red), recovered with one interstitial uranium defect (Six oxygen ions are good examples of distortion type defects [1]). This critical point and above in the linear behaviour as swelling occur due to radiation corresponds to the first stage of thermal recovery. Presumably, both oxygen and uranium defects are recovered, but many more oxygen ions are recovered in the first stage. The recovery process is initialized by the migration of the interstitial uranium ion to the vacant position despite being the defect minority. Thus, determining the defects attributed to a recovery stage by measuring the activation energy is questionable because the majority of recovered defects in the first stage are oxygens but the activation energy needed to initiate that process is associated to uranium ion recovery.

Supplementary video related to this article can be found at http://dx.doi.org/10.1016/j.jallcom.2017.07.100.

The proposed mechanism for the first stage can be verified by analysing Fig. 6. The first stage of recovery is observed for the 40 uranium IFP and 70 uranium IFP samples, whereas the first stage of recovery was absent for the 20 uranium IFP sample. Referring to Figs. 10 and 11 in the previous study [1], the 20 uranium IFP sample is below the critical point in linear behaviour, where the uranium

interstitial octahedral cages do not contain oxygen ions. In the second and third stages, only uranium ion obstruction defects are recovered. In the literature, the recovery stages for α-particle-irradiated uranium dioxide crystals are oxygen interstitials, uranium vacancies, and helium ions trapped in vacancies for the first, second, and third stages, respectively, which is partly similar to our results: uranium-oxygen, uranium and uranium interstitials. The experimental results can be interpreted as: oxygen migration in the first and helium migration in the last stage are a corollary of the recovered uranium ions migrating from an octahedral cage to a vacancy point via interstitialcy mechanism.

5. Conclusion

In this study, the thermal recovery mechanism of irradiated uranium dioxide was investigated by classical MD simulation and by DFT. The activation and recovery energies, migration energy barrier, lattice parameter change, and defects attributed to each recovery stages were obtained. Both computational methods and the experimental results are in agreement. In addition, the recovery mechanisms were interpreted with the visualization of the simulated data and defects related to each recovery stages are obtained. Finally, future studies could involve other actinide dioxides, since they also display three recovery stages [7], which could indicate similarities in the defects at each recovery stage.

Acknowledgements

Computing resources used in this work were partially provided by the National Center for High Performance Computing of Turkey (UHeM) under grant number 5003802015. The numerical calculations reported in this paper were partially performed at TUBITAK ULAKBIM, High Performance and Grid Computing Center (TRUBA resources).

References

[1] S.D. Günay, Swelling mechanisms of UO_2 lattices with defect ingrowths, PLoS One 10 (2015) e0134500.
[2] N. Nakae, A. Harada, T. Kirihara, S. Nasu, Irradiation induced lattice defects in UO_2, J. Nucl. Mater 71 (1978) 314–319.
[3] N. Nakae, T. Kirihara, S. Nasu, Irradiation induced volume change in UO_2, J. Nucl. Mater 74 (1978) 1–9.
[4] W.J. Weber, Ingrowth of lattice defects in alpha irradiated UO_2 single crystals, J. Nucl. Mater 98 (1981) 206–215.
[5] N. Nakae, Y. Iwata, T. Kirihara, Thermal recovery of defects in neutron irradiated UO_2, J. Nucl. Mater 80 (1979) 314–322.
[6] W.J. Weber, Thermal recovery of lattice defects in alpha-irradiated UO_2 crystals, J. Nucl. Mater 114 (1983) 213–221.
[7] M. Kato, A. Komeno, H. Uno, H. Sugata, N. Nakae, K. Konashi, M. Kasimura, Self-radiation damage in plutonium and uranium mixed dioxide, J. Nucl. Mater 393 (2009) 134–140.
[8] H. Matzke, Radiation damage in crystalline insulators, oxides and ceramic nuclear fuels, Radiat. Eff. 64 (1982) 3–33.
[9] H. Kim, M.H. Kim, M. Kaviany, Lattice thermal conductivity of UO_2 using ab-initio and classical molecular dynamics, J. Appl. Phys. 115 (2014), 123510-1–123510–7.
[10] B. Dorado, B. Amadon, M. Freyss, M. Bertolus, DFT+U calculations of the ground state and metastable states of uranium dioxide, Phys. Rev. B 79 (2009), 235125-1–235125–8.
[11] M. Iwasawa, Y. Chen, Y. Kaneta, T. Ohnuma, H.-Y. Geng, M. Kinoshita, First-principles calculation of point defects in uranium dioxide, Mater. Trans. 47 (2006) 2651–2657.
[12] E. Yakub, C. Ronchi, D. Staicu, Molecular dynamics simulation of premelting and melting phase transitions in stoichiometric uranium dioxide, J. Chem. Phys. 127 (2007), 094508-1–094508–11.
[13] M.W.D. Cooper, M.J.D. Rushton, R.W. Grimes, A many-body potential approach to modelling the thermomechanical properties of actinide oxides, J. Phys. Condens. Matter 26 (2014) 105401.
[14] R. Devanathan, J. Yu, W.J. Weber, Energetic recoils in UO_2 simulated using five different potentials, J. Chem. Phys. 130 (2009), 174502-1–174502–9.
[15] K. Refson, Moldy: a portable molecular dynamics simulation program for serial and parallel computers, Comput. Phys. Commun. 126 (2000) 310–329.
[16] S. Plimpton, Fast parallel algorithms for short-range molecular dynamics, J. Comput. Phys. 117 (1995) 1–19.
[17] H. Blank, Plutonium 1975 and Other Actinides, North-Holland Pub. Co.; American Elsevier Pub. Co., Amsterdam, 1976, p. 873.
[18] D. Vollath, Plutonium 1975 and Other Actinides, North-Holland Pub. Co.; American Elsevier Pub. Co., Amsterdam, 1976, p. 843.
[19] A.C. Damask, G.J. Dienes, Point Defects in Metals, Ch. 3, Gordon and Breach, New York, 1963, p. 145.
[20] W. Primak, Kinetics of processes distributed in activation energy, Phys. Rev. 100 (1955) 1677–1689.
[21] W. Primak, H. Szymanski, Radiation damage in vitreous silica: annealing of the density changes, Phys. Rev. 101 (1956) 1268–1271.
[22] W. Primak, Annealing of radiation damage in graphite, J. Appl. Phys. 49 (1978) 4761–4764.
[23] G. Kresse, J. Hafner, Ab initio molecular dynamics for liquid metals, Phys. Rev. B 47 (1993) 558–561.
[24] G. Kresse, J. Furthmüller, Efficiency of ab-initio total energy calculations for metals and semiconductors using a plane-wave basis set, Comput. Comput. Mater. Sci. 6 (1996) 15–50.
[25] G. Kresse, J. Furthmüller, Efficient iterative schemes for ab initio total-energy calculations using a plane-wave basis set, Phys. Rev. B 54 (1996) 11169–11186.
[26] G. Henkelman, B.P. Uberuaga, H. Jónsson, A climbing image nudged elastic band method for finding saddle points and minimum energy paths, J. Chem. Phys. 113 (2000) 9901–9904.
[27] D. Sheppard, P. Xiao, W. Chemelewski, D.D. Johnson, G. Henkelman, A generalized solid-state nudged elastic band method, J. Chem. Phys. 136 (2012), 074103-1–074103–8.
[28] B. Dorado, D.A. Andersson, C.R. Stanek, M. Bertolus, B.P. Uberuaga, G. Martin, M. Freyss, P. Garcia, First-principles calculations of uranium diffusion in uranium dioxide, Phys. Rev. B 86 (2012), 035110-1–035110–10.